A&A 377, 442–449 (2001)
DOI: 10.1051/0004-6361:20011142

Astronomy & Astrophysics

Deep BVR photometry of the Chandra Deep Field South from the COMBO-17 survey⋆

C. Wolf[1], S. Dye[1,2], M. Kleinheinrich[1], K. Meisenheimer[1], H.-W. Rix[1], and L. Wisotzki[3]

[1] Max-Planck-Institut für Astronomie, Königstuhl 17, 69117 Heidelberg, Germany
[2] Astrophysics Group, Blackett Lab, Imperial College, Prince Consort Road, London, UK
[3] Institut für Physik, Universität Potsdam, Am Neuen Palais 10, 14469 Potsdam, Germany

Received 22 December 2000 / Accepted 26 July 2001

Abstract. We report on deep multi-color imaging ($R_{5\sigma} = 26$) of the Chandra Deep Field South, obtained with the Wide Field Imager (WFI) at the MPG/ESO 2.2 m telescope on La Silla as part of the multi-color survey COMBO-17. As a result we present a catalogue of 63 501 objects in a field measuring $31\farcm5 \times 30'$ with astrometry and BVR photometry. A sample of 37 variable objects is selected from two-epoch photometry. We try to give interpretations based on color and variation amplitude.

Key words. techniques: image processing – techniques: photometric – surveys – catalogs – quasars: general

1. Introduction

Deep fields have become a favourite tool of observational cosmology, particularly in conjunction with the construction of multiwavelength datasets. Besides the ubiquitous Hubble Deep Fields, another illustrative example is the ROSAT Deep Survey in the Lockman Hole (Hasinger et al. 1998) and its optical follow-up by imaging and spectroscopy (e.g., Schmidt et al. 1998). However, full spectroscopic coverage is usually impossible to obtain, and the reconstruction of distances often has to rely on photometric redshift estimation. Despite major advances in this area, there is always a certain degree of degeneracy between object classes, such as different galaxy types, and their redshifts. Breaking this degeneracy is possible only by incorporating independent spectroscopic information, such as adding infrared colors or moving towards finer spectrophotometric resolution.

Wolf et al. (2001a,b) demonstrated that the use of medium-band filters leads to a substantial gain in classification accuracy and discriminative power, as compared to simple broad-band photometry. In 1999 we initiated a new multicolor survey using the Wide Field Imager (WFI, Baade et al. 1998, 1999) at the MPG/ESO 2.2 m telescope on La Silla, Chile. The survey was designed to make full use of the capabilities offered by the WFI and at the same time exploit the experience collected in the course of earlier multicolor projects. By incorporating 17 different optical filters into our new survey the COMBO-17 (*Classifying Objects by Medium-Band Observations in 17 filters*) project goes a major step beyond the traditional multicolor approach. It permits confident spectral classification of objects with $R \lesssim 24$ into stars, galaxies, quasars, and the recognition of exotic objects, and it facilitates accurate subclassification, redshifts estimation, and SED reconstruction for galaxies and quasars. The survey area comprised four independent WFI fields amounting to a total area of 1 deg^2. Overall objectives of COMBO-17 are:

- The galaxy catalogue will be complete to $R < 24$ and contain ∼50 000 galaxies with accurate redshifts and spectral classification up to $z \simeq 1.5$, to be used to study the evolution of the galaxy luminosity function and clustering properties;
- The quasar sample will contain ∼500 QSOs, with nearly uniform completeness over the redshift range $0.5 \lesssim z \lesssim 5$, well suited to trace the turnover in QSO evolution;
- Deep high-resolution R-band images with $0\farcs75$ $FWHM$ permit morphological classification and gravitational lensing studies.

In this paper we focus on the "Chandra Deep Field South" (Giacconi et al. 2000) subject to a deep X-ray exposure by the Chandra satellite observatory and target of a wide range of multiwavelength studies from several groups. It is particularly worth noting that the COMBO-17 field

Send offprint requests to: C. Wolf,
e-mail: cwolf@mpia-hd.mpg.de

⋆ Complete Table 2 is only available in electronic form at the CDS via anonymous ftp to cdsarc.u-strasbg.fr (130.79.128.5) or via
http://cdsweb.u-strasbg.fr/cgi-bin/qcat?J/A+A/377/442

Table 1. Observing log for B, V and R exposures on the Chandra Deep Field South as part of the COMBO-17 survey.

Epoch (UT)	Band	Seeing	Exposure (s)
1999, Oct. 10	V	$1\farcs0 \ldots 1\farcs4$	$14 \times 600 + 3 \times 20$
1999, Oct. 13	B	$1\farcs0 \ldots 1\farcs4$	$10 \times 500 + 3 \times 20$
1999, Oct. 19	R	$0\farcs6 \ldots 0\farcs9$	25×420
1999, Oct. 20	R	$0\farcs6 \ldots 0\farcs9$	$11 \times 420 + 1 \times 370$
2000, Feb. 6	R	$0\farcs6 \ldots 0\farcs9$	$6 \times 500 + 2 \times 60$
2000, Feb. 8	R	$0\farcs6 \ldots 0\farcs9$	$10 \times 500 + 1 \times 200$

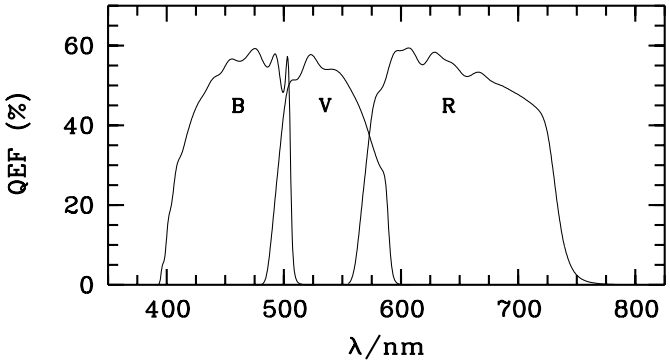

Fig. 1. Total system efficiencies for the WFI filters B, V and R (including telescope, instrument and detector).

of view contains the Chandra field entirely facilitating the efficient combination of optical and X-ray data. In this paper, we present a first catalogue of optically selected sources down to R-band magnitudes of $R \lesssim 26$. This catalogue is publically available over the world-wide web.

2. Observations

We have imaged the Chandra Deep Field South in all 17 filters for the COMBO-17 project using the Wide Field Imager (WFI, Baade et al. 1998, 1999) at the MPG/ESO 2.2 m telescope on La Silla, Chile. The WFI is a mosaic camera consisting of eight 2k × 4k CCDs with ∼67 million pixels in total, a pixel scale of $0\farcs238$ and a field of view of $33' \times 34'$. The CCDs are rather blue sensitive and some of them are cosmetically suboptimal since they are only of engineering grade.

Here we discuss data obtained in the broad-band WFI filters B, V and R (see Table 1 for a brief observing log). Our data encompass a total exposure time of 5000 s in B and 8400 s in V with seeing on the order of $\sim 1\farcs2$ and altogether 23 700 s in R with $\sim 0\farcs75$ mean PSF. Besides long exposures for efficient light gathering, we included short exposures for the photometry of brighter objects, in particular to avoid saturation of our brighter standard stars.

The long exposures followed a dither pattern with ten telescope pointings spread by $\Delta\alpha, \Delta\delta < \pm 72''$. This dither pattern is motivated by the intent to close the gaps in the CCD mosaic, but limited by the requirement of keeping field rotation at a minimum. Due to the gaps in the CCD mosaic the effective exposure time varies within the field. However, dithering was performed such, that each position on the sky falls onto a CCD in at least eight out of ten exposures, while 97% of the area is always recorded in every image.

Twilight flatfields were obtained with offsets of $10''$ between consecutive exposures. Exposure times ranged between 0.5 and 100 s per frame (note that the WFI shutter design allows exposures as short as 0.1 s without causing significant spatial variations in the illumination across the CCD mosaic (Wackermann 1999).

We have established our own set of tertiary standard stars based on *spectrophotometric* observations, mainly in order to achieve a homogeneous photometric calibration for all 17 WFI filter bands. Two stars of spectral types G–F and magnitudes $B_J \simeq 16$ were selected in each COMBO-17 field, drawn from the Hamburg/ESO Survey database of digital objective prism spectra (Wisotzki et al. 2000). The spectrophotometric observations for the Chandra Deep Field South were conducted at La Silla on Oct. 25, 1999, using the Danish 1.54 m telescope equipped with DFOSC. A wide ($5''$) slit was used for the COMBO-17 standards as well as for the external calibrator, in this case the HST standard HD 49 798 (Bohlin & Lindler 1992). Two exposures of 45 min were taken of each star, one with the blue-sensitive grism 4 covering the range $\lambda = 3400$–7400 Å, and one with the red-sensitive grism 5 covering $\lambda > 5200$ Å.

The spectra were reduced by standard procedures and have a final signal-to-noise ratio of >30 per pixel except very near to the low- and high-wavelength cutoffs. The agreement between spectra in the substantial overlap in wavelength between the two grisms is excellent, confirming that contamination from second order was negligible. The absolute spectrophotometric accuracy, estimated from comparing several spectra of the external calibrator HD 49 798 obtained during the entire observing run, is better than 10%.

3. Data reduction

All procedures used for the data reduction are based on the MIDAS package and are routinely used at MPIA. An image processing pipeline has been developed specifically for dithered WFI survey images by us. It makes intensive use of programmes developed by Meisenheimer, Röser and Hippelein for the Calar Alto Deep Imaging Survey (CADIS). The pipeline performes basic image reduction and includes standard operations of bias subtraction, CCD non-linearity correction, flatfielding, masking of hot pixels and bad columns, cosmic correction and subsequent stacking into a deep co-added frame covering the area that is common to all frames ($31\farcm5 \times 30'$). Details on the processing will be given in a forthcoming paper when the data reduction has been completed for all filters and fields (Meisenheimer et al., in preparation).

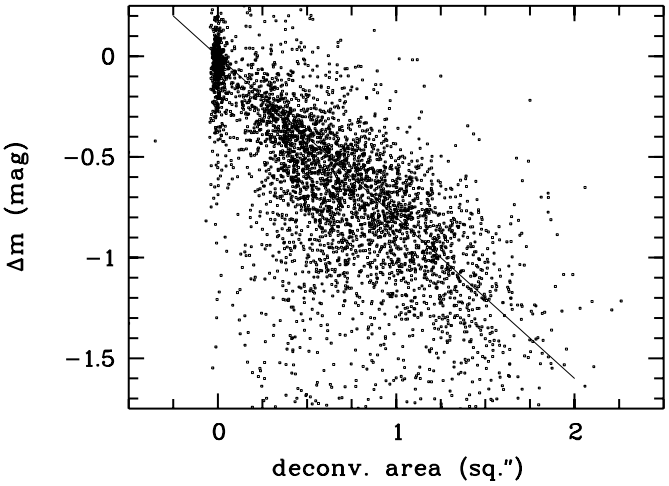

Fig. 2. Distribution of aperture correction magnitudes versus deconvolved area of bright objects. Stars are at zero level while extended objects reach down to negative values. The straight line shows the best fit to the data which has been adopted for a general aperture correction that is also applied to faint objects.

The co-added frame thus obtained is not optimal for photometry since the flux errors are not sufficiently described by photon noise only. Instead, flatfield errors and other systematic effects which are locally changing on the CCD can only be incorporated into the error analysis by measuring the photometry on the individual frames, where the object location varies due to dithering. Combining these individual measurements allows to derive flux errors from the scatter among the frames.

The deep co-added images we in fact only used for object search and visual inspection purposes. Objects have been searched only on the *R*-band sum frame, which provides a uniform, sharp PSF with $0\farcs75$ *FWHM* and the best signal-to-noise ratio for almost all known kinds of objects expected in the field. We used the SExtractor software (Bertin & Arnouts 1996) with the recommended default setups in the parameter file, except for choosing a minimum of 12 significant pixels required for the detection of an object. We first search rather deep and then clean the list of found objects from those having more than $0\fm333$ error in the SExtractor best-guess magnitude. As a result we obtained a catalogue of 63 501 objects with positions and morphology. Starting from the known object positions on the co-added *R*-band frame, we transform the positions of the objects onto every single frame and measure their fluxes on them.

COMBO-17 is a spectrophotometric survey, where color indices are the prime observables entering a process of classification and redshift estimation later. Therefore, it is necessary to choose an optimum way to measure these indices. For ground-based observations it is important to avoid that variable observing conditions introduce offsets between bands when the observations are taken sequentially. Variable seeing, e.g., might influence the flux measurement of star-like and extended objects in a different way.

This requires us to assess the seeing point spread function on every frame very carefully. Then, we essentially convolve each image to a common *effective* point spread function and measure the central surface brightness of each object in a weighted circular aperture (Röser & Meisenheimer 1991). This has the disadvantage that the spatial resolution (i.e. the minimum separation of objects neighboring each other) is limited by the frame with the poorest seeing. Especially, we do not attempt to separate the fluxes among closely blended objects. For the context of this paper we use an effective PSF of $1\farcs5$.

The flux calibration is performed by identifying our spectrophotometric standard stars and convolving their spectra with the total system efficiency in the given filter (see Fig. 1). We then know the physical photon flux we have to assign to them, and establish the flux scale for all objects. Since the spectra of the standard stars have been measured with a $5''$ wide slit in good seeing, we are confident that we have collected basically all their light. This implies that the photometry of all stars should be accurate since the standard stars are measured with the same aperture in the images as all other objects.

Extended objects however have their fluxes underestimated and therefore we performed a set of photometric runs with apertures increasing in steps to $10''$ and no weighting functions. At $10''$ diameter basically all fluxes have already converged allowing us to measure total magnitudes for virtually all objects except for a few very large and bright galaxies. This total magnitude can not be measured for the fainter objects since the background noise from the large aperture would be extremely high. Therefore, we measured the magnitude difference between the total magnitude and our small weighted circular aperture for the bright objects and derived an aperture correction function depending on morphological parameters (see Fig. 2). This function provides an estimated aperture correction and is uniformly applied to all objects (see Fig. 5).

The fluxes from individual frames are averaged into a final flux for each object with the error being derived from the scatter. This way, the error does not only take photon noise into account, but further sources of error, such as imperfect flatfielding and uncorrected CCD artifacts. However, we prevent chance coincidences of count rates from pretending unreasonably low errors by using the errors derived from background and photon noise as a lower limit (see Meisenheimer et al., in preparation, for a full discussion of the photometric analysis).

4. The catalogue and initial results

The object catalogue derived from the observations presented contains positions and *BVR* photometry of 63 501 objects selected in *R* within a field of $31\farcm5 \times 30'$ size. The depth and the seeing quality of our *R*-band imaging makes this catalogue

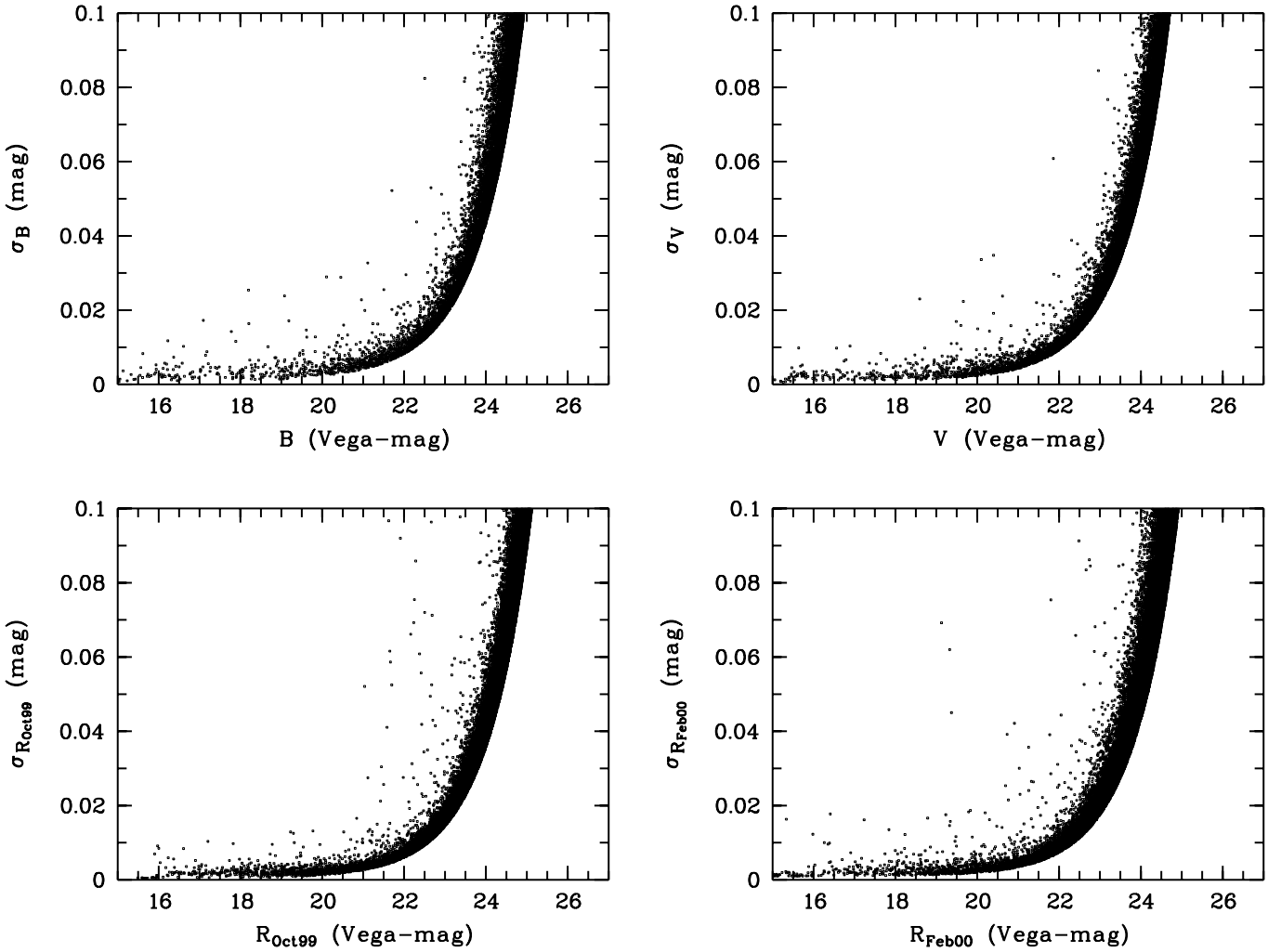

Fig. 3. Errors versus magnitudes for all objects with errors below $0\overset{\mathrm{m}}{.}1$ observed in the WFI filters B, V and R (two epochs).

Table 2. Format of the object catalogue made available at CDS.

Label	Explanation
Seq	Sequential number
RA	Right ascension (J2000), internal accuracy $\pm 0\overset{''}{.}15$
DE	Declination (J2000), internal accuracy $\pm 0\overset{''}{.}15$
$B_{\rm mag}$	Aperture magnitude, scaled to total flux for stars
$e-B_{\rm mag}$	Mean error (sigma) of $B_{\rm mag}$
$V_{\rm mag}$	Aperture magnitude, scaled to total flux for stars
$e-V_{\rm mag}$	Mean error (sigma) of $V_{\rm mag}$
$R_{\rm mag}$	Aperture magnitude, scaled to total flux for stars
$e-R_{\rm mag}$	Mean error (sigma) of $R_{\rm mag}$
$ApC_{\rm mag}$	Estimated correction from aperture to total mag.

potentially very useful for the scientific community. Therefore, the catalogue (format see Table 2) is available to the public at Centre de Données astronomiques de Strasbourg (CDS, `http://cdsweb.u-strasbg.fr/cgi-bin/qcat?J/A+A/377/442`) and on the COMBO-17 survey homepage at MPIA (`http://www.mpia.de/COMBO/`). In the following we discuss data quality issues and present a first sample of variable objects identified from the two epochs of R-band observations.

The quality of our photometry differs for point sources and extended sources. Essentially, it is a seeing-adaptive central surface brightness measurement giving accurate fluxes for point sources while underestimating the total flux of extended sources. But since it is performed on the individual frames in an optimal seeing-adaptive fashion, it yields more accurate colors and estimates the errors more realistically than measurements on a single co-added frame.

Figure 3 shows the photometric errors versus magnitudes of all objects we measured at less than $0\overset{\mathrm{m}}{.}1$ error. The photon noise limit can be seen as a sharp parabolic edge to the right of the object clouds. We use magnitude histograms of objects with errors of $\sim$10% to assess a representative 10-σ magnitude limit for point-source photometry. In Fig. 4 we can see that all R-band images combined reach $R_{\rm lim,10\sigma} = 25.25$ which is $R_{\rm lim,5\sigma} = 26.00$.

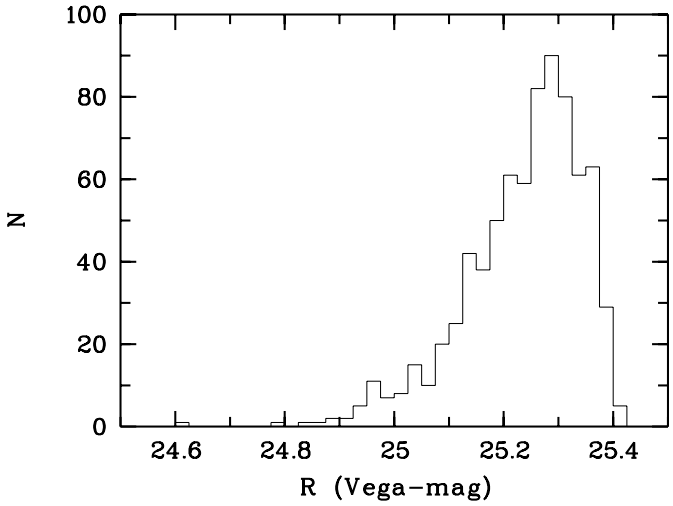

Fig. 4. R-band histogram of objects with errors of ∼10% from combined photometry of both observing runs. From this distribution we read the 10σ limiting magnitude as the median at $R = 25\overset{\mathrm{m}}{.}25$.

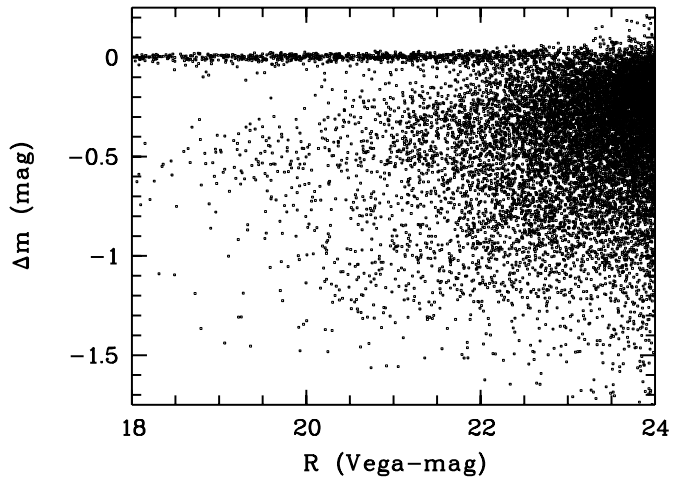

Fig. 5. Distribution of aperture correction magnitudes versus R magnitude. Stars are at zero level while extended objects reach down to negative values.

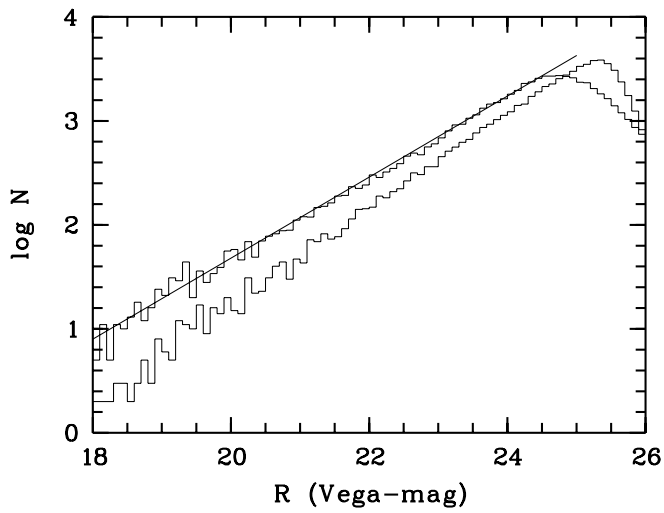

Fig. 6. Number counts histogram of all objects excluding stellar objects with $R < 23$. The lower staircase line is based on the aperture magnitude which is accurately calibrated for point sources. The upper staircase line is based on total magnitudes corrected for aperture effects, while the straight black line with a slope of 0.39 has been fitted to the latter staircase distribution. Note, that this plot contains ∼60 000 objects and shows their counts in bins of $0\overset{\mathrm{m}}{.}1$.

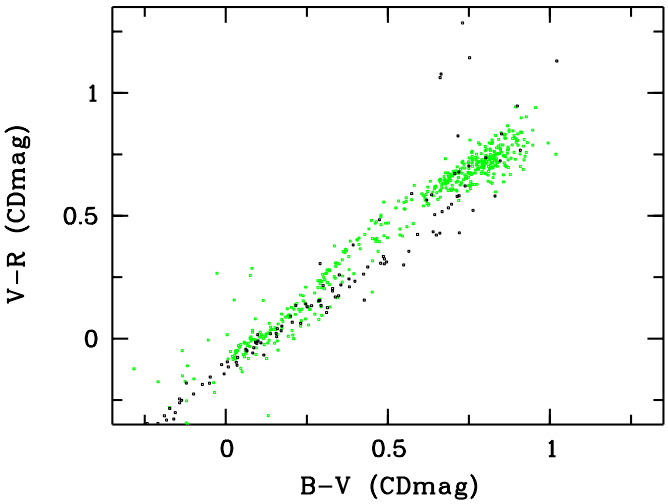

Fig. 7. $B-V$ and $V-R$ colors of observed stars compared to template colors. Shown are bright point sources from the object catalogue ($R = 17 \ldots 21$, grey dots) and colors for the Pickles (1998) spectral library (black dots). Most stars in our field belong to the halo population, while most of the Pickles library are nearby stars from the disk population. The populations form two arms that are clearly separated for G and K stars ($B - V \approx 0.3 \ldots 0.6$). We note a number of blue objects off the main sequence, which are probably quasars passing this purely morphological selection. The units of the colors are photon count color indices (CD_{mag}) as in Wolf et al. (2001), see also text.

However, the fluxes of extended objects are approximated by an aperture correction. The median correction among extended objects amounts to $\sim -0\overset{\mathrm{m}}{.}5$ (see Fig. 5). Figure 6 shows a number counts histogram for the aperture magnitude as well as for the corrected total magnitude excluding point sources at $R < 23$. The counts in aperture magnitude suggest that our object list is at least complete to $R > 25$ in terms of point-source photometry. The counts of total magnitude suggest completeness among galaxies provided to at least $R \approx 24.5$. With a slope of ∼0.39 the counts are consistent with galaxy counts from the literature. However, a detailed discussion of the counts is beyond the scope of this paper.

We checked our flux calibration by comparing measured colors of stellar objects with those predicted by synthetic photometry. We convolved the Pickles (1998) library of stellar spectra with the total efficiency curves of our filters and plotted their $B-V$ and $V-R$ colors as black dots in Fig. 7. Our own point sources are overplotted as grey dots and agree with the expected colors without any further correction. Shown are photon count color

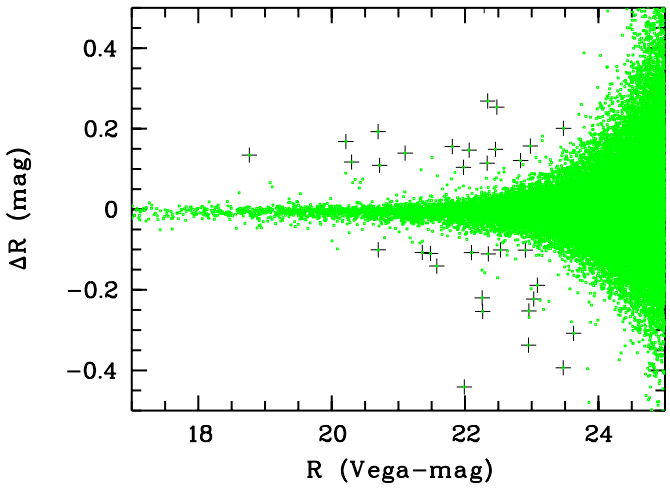

Fig. 8. *R*-band magnitude difference between the two epochs October 1999 and February 2000 versus combined *R*-magnitude (grey dots = all objects). Objects selected as variable are shown as black crosses, but strongly variable sources lie outside the plot. Twenty objects have been omitted from the sample after visual inspection since they were affected by scattered light or diffraction spikes of 9th magnitude stars.

indices in units of $CD_{\rm mag}$ defined by Wolf et al. (2001b). As a physical magnitude definition besides $AB_{\rm mag}$ and $ST_{\rm mag}$ the $CD_{\rm mag}$ is

$$CD_{\rm mag} = -2.5 \log F_{\rm phot} + 20\overset{\rm m}{.}01 \quad \text{with } F_{\rm phot} \text{ in } \gamma\,{\rm m}^{-2}\,{\rm s}^{-1}\,{\rm nm}^{-1}, \tag{1}$$

and matches the common magnitude zeropoint of (astronomical) Vega-mag, $AB_{\rm mag}$ and $ST_{\rm mag}$ at $\lambda_0 = 548$ nm.

We note that most stars observed in our field belong to the halo population, while most stars in the Pickles library are nearby stars from the disk population. The populations form two arms that are separated for G/K stars ($B - V_{\rm CD} \approx 0.3 \ldots 0.6$) and have quite different relative population densities in the data and the library. We also note a few blue objects off the main sequence, which are most likely quasars passing the purely morphological selection used here.

5. A first set of variable objects

For variability studies we calculated a magnitude change between the two epochs October 1999 and February 2000 and a related error as:

$$\Delta R = R_{\rm Feb00} - R_{\rm Oct99}, \tag{2}$$

and

$$\sigma_{\Delta R} = \sqrt{\sigma^2_{R_{\rm Oct99}} + \sigma^2_{R_{\rm Feb00}}}. \tag{3}$$

Figure 8 shows the magnitude difference of all objects with $R < 25$ versus the combined *R*-magnitude. The distribution underlines that the photometric errors are realistic and the photometry is essentially consistent among the two epochs.

We selected a first sample of variable objects using the following criteria:

1. faint cutoff: at least one detection must have $R < 24$;
2. absolute variability threshold: $\Delta R > 0.1$;
3. variability significance threshold: $\Delta R/\sigma_{\Delta R} > 5$.

This way 57 entries are selected in the catalogue which were made subject to visual inspection on the sum frames of the two epochs. We eliminated 20 faint objects from the sample which were affected by scattered light or diffraction spikes of 9th magnitude stars. We have confidence in the variability of the remaining 37 objects and list their positions and original photometry from the two epochs in Table 3. The number of variable objects increases strongly with fainter magnitude but faintwards of $R \sim 22.5$ the significance criterion becomes stronger than the absolute threshold, thereby reducing the numbers again. The published catalogue of course provides the possibility to identify objects with a smaller amplitude of variability.

We show the location of the variables in a $(B-V)$ vs. $(V-R)$ color diagram in Fig. 9. The red magnitude is here only taken from October 1999 images to keep the color indices free of skewing by long-term variability. The October frames have been taken during 9 days, so short-term variability could still have changed the color indices, especially for RR Lyrae stars given their typical periods of ∼1 day. Also shown are expected colors for stars from the Pickles atlas (compare with Fig. 7) and for a quasar color library derived from quasar spectra modelled for $z = 0 \ldots 6$ as a combination of power-law spectra, an emission-line contour (Francis et al. 1991) and Lyman-forest.

If we assume an absence of short-term variability, we would classify most objects as quasars or Seyfert galaxies, while a few could be stars. Of course, the stellar sample could contain some RR Lyrae stars whose variability time scale of ∼1 day could offset their colors. These color offsets could move the stars in any directions (+/−) along any of the color axes with equal probability, and a scattered sample should appear with a comparable fraction of stars below and above the original color sequence.

In Fig. 9 we see that only three objects show up below the stellar sequence, while ∼30 are located above. Therefore we conclude that most of the variable objects presented are indeed quasars while some objects are Seyfert-I galaxies where bright host galaxies dominate the colors. The COMBO-17 group has meanwhile reduced all data on the Chandra field and prepared lists of stars, galaxies and quasars at $R \lesssim 24$, which are analysed in forthcoming papers.

Among the variable objects are also three candidates for Supernovae (see Table 3), which had their bright phase in October 1999 and are undetectable to visual inspection in the February co-added frame. The first two showed up as a significant off-center brightening of a tiny faint galaxy (objects 16 404 and 52 103 in Table 3).

The third candidate has a rather red $B-V$ color (object 36 683 in Table 3). It is a point source located only 2.″0 North and 0.″9 East of a small galaxy with

Table 3. A first sample of variable objects drawn from *R*-band photometry of two epochs. While most objects are likely to be quasars at $z < 3$, some objects might be Seyfert galaxies or even stars. We marked the objects where we assume a Supernova has caused the variability. The object numbers refer to the published catalog and the object names encode the object positions.

cat. No.	object name	$\alpha_{\rm J2000}$	$\delta_{\rm J2000}$	$B_{\rm Oct99}$	$V_{\rm Oct99}$	$R_{\rm Oct99}$	$R_{\rm Feb00}$	comment
4050	COMBO–0332203−280215	$03^{\rm h}32^{\rm m}20\overset{\rm s}{.}315$	$-28°02'14\overset{''}{.}66$	21.146	21.013	20.698	20.605	
4427	COMBO–0331278−280156	$03^{\rm h}31^{\rm m}27\overset{\rm s}{.}766$	$-28°01'55\overset{''}{.}96$	24.537	24.213	23.084	22.903	
4809	COMBO–0331362−280150	$03^{\rm h}31^{\rm m}36\overset{\rm s}{.}247$	$-28°01'49\overset{''}{.}59$	22.695	22.525	22.258	22.046	
5826	COMBO–0332470−280119	$03^{\rm h}32^{\rm m}46\overset{\rm s}{.}953$	$-28°01'19\overset{''}{.}38$	24.805	23.736	22.906	22.812	
7139	COMBO–0332354−280041	$03^{\rm h}32^{\rm m}35\overset{\rm s}{.}368$	$-28°00'41\overset{''}{.}19$	24.338	24.225	23.629	23.328	
7902	COMBO–0332302−280020	$03^{\rm h}32^{\rm m}30\overset{\rm s}{.}200$	$-28°00'19\overset{''}{.}95$	22.308	21.901	21.809	21.972	
13 244	COMBO–0333148−275749	$03^{\rm h}33^{\rm m}14\overset{\rm s}{.}849$	$-27°57'48\overset{''}{.}96$	23.992	24.026	23.473	23.087	
15 278	COMBO–0331208−275649	$03^{\rm h}31^{\rm m}20\overset{\rm s}{.}762$	$-27°56'48\overset{''}{.}97$	20.983	20.829	20.719	20.835	
15 396	COMBO–0332161−275644	$03^{\rm h}32^{\rm m}16\overset{\rm s}{.}133$	$-27°56'44\overset{''}{.}12$	23.064	22.916	22.533	22.440	
16 155	COMBO–0332042−275626	$03^{\rm h}32^{\rm m}04\overset{\rm s}{.}157$	$-27°56'26\overset{''}{.}39$	24.130	23.860	23.029	22.814	
16 404	COMBO–0332226−275622	$03^{\rm h}32^{\rm m}22\overset{\rm s}{.}604$	$-27°56'22\overset{''}{.}48$	24.001	23.360	22.339	22.616	SN candidate
20 787	COMBO–0333053−275409	$03^{\rm h}33^{\rm m}05\overset{\rm s}{.}312$	$-27°54'09\overset{''}{.}11$	22.525	21.951	21.576	21.442	
27 080	COMBO–0333042−275103	$03^{\rm h}33^{\rm m}04\overset{\rm s}{.}206$	$-27°51'02\overset{''}{.}77$	24.619	23.535	22.332	22.455	
28 275	COMBO–0331525−275027	$03^{\rm h}31^{\rm m}52\overset{\rm s}{.}508$	$-27°50'27\overset{''}{.}48$	24.062	23.586	22.456	22.613	
29 793	COMBO–0333104−274945	$03^{\rm h}33^{\rm m}10\overset{\rm s}{.}389$	$-27°49'44\overset{''}{.}75$	24.112	23.775	23.202	22.051	
30 792	COMBO–0332432−274914	$03^{\rm h}32^{\rm m}43\overset{\rm s}{.}239$	$-27°49'14\overset{''}{.}11$	22.442	22.474	22.288	22.801	
32 254	COMBO–0333263−274831	$03^{\rm h}33^{\rm m}26\overset{\rm s}{.}301$	$-27°48'31\overset{''}{.}14$	23.329	23.352	22.957	22.712	
34 357	COMBO–0332087−274734	$03^{\rm h}32^{\rm m}08\overset{\rm s}{.}669$	$-27°47'34\overset{''}{.}20$	19.422	19.141	18.765	18.907	
35 677	COMBO–0332142−274647	$03^{\rm h}32^{\rm m}14\overset{\rm s}{.}246$	$-27°46'47\overset{''}{.}44$	24.293	24.051	23.477	23.685	
36 683	COMBO–0333343−274621	$03^{\rm h}33^{\rm m}34\overset{\rm s}{.}343$	$-27°46'20\overset{''}{.}94$	25.560	23.748	23.329	25.408	SN candidate
37 487	COMBO–0332391−274602	$03^{\rm h}32^{\rm m}39\overset{\rm s}{.}084$	$-27°46'01\overset{''}{.}82$	21.101	20.944	20.696	20.897	
38 551	COMBO–0332300−274530	$03^{\rm h}32^{\rm m}29\overset{\rm s}{.}982$	$-27°45'29\overset{''}{.}84$	21.692	21.480	21.102	21.249	
38 905	COMBO–0333036−274519	$03^{\rm h}33^{\rm m}03\overset{\rm s}{.}616$	$-27°45'18\overset{''}{.}71$	23.744	23.362	22.833	22.962	
39 432	COMBO–0332302−274505	$03^{\rm h}32^{\rm m}30\overset{\rm s}{.}218$	$-27°45'04\overset{''}{.}54$	22.545	22.344	21.977	22.089	
41 159	COMBO–0332109−274415	$03^{\rm h}32^{\rm m}10\overset{\rm s}{.}924$	$-27°44'14\overset{''}{.}73$	23.073	22.931	22.350	22.247	
41 247	COMBO–0331534−274412	$03^{\rm h}31^{\rm m}53\overset{\rm s}{.}360$	$-27°44'12\overset{''}{.}11$	24.048	23.752	22.952	22.622	
41 776	COMBO–0333358−274400	$03^{\rm h}33^{\rm m}35\overset{\rm s}{.}841$	$-27°44'00\overset{''}{.}07$	23.408	23.287	22.981	23.145	
42 601	COMBO–0332591−274340	$03^{\rm h}32^{\rm m}59\overset{\rm s}{.}067$	$-27°43'39\overset{''}{.}53$	22.463	22.176	21.482	21.380	
43 151	COMBO–0332004−274319	$03^{\rm h}32^{\rm m}00\overset{\rm s}{.}365$	$-27°43'19\overset{''}{.}45$	22.726	22.436	22.062	22.216	
46 562	COMBO–0332479−274148	$03^{\rm h}32^{\rm m}47\overset{\rm s}{.}915$	$-27°41'47\overset{''}{.}88$	23.254	22.887	22.096	21.996	
47 501	COMBO–0331187−274121	$03^{\rm h}31^{\rm m}18\overset{\rm s}{.}698$	$-27°41'21\overset{''}{.}30$	22.768	22.291	21.989	21.556	
48 870	COMBO–0333289−274044	$03^{\rm h}33^{\rm m}28\overset{\rm s}{.}941$	$-27°40'43\overset{''}{.}68$	22.550	22.537	22.477	22.738	
52 103	COMBO–0331256−273908	$03^{\rm h}31^{\rm m}25\overset{\rm s}{.}611$	$-27°39'08\overset{''}{.}48$	25.298	24.421	23.274	24.475	SN candidate
52 280	COMBO–0333211−273912	$03^{\rm h}33^{\rm m}21\overset{\rm s}{.}079$	$-27°39'11\overset{''}{.}92$	20.691	20.529	20.212	20.388	
57 527	COMBO–0333184−273641	$03^{\rm h}33^{\rm m}18\overset{\rm s}{.}358$	$-27°36'41\overset{''}{.}34$	22.785	22.331	21.360	21.260	
58 758	COMBO–0333037−273611	$03^{\rm h}33^{\rm m}03\overset{\rm s}{.}722$	$-27°36'10\overset{''}{.}90$	20.924	20.755	20.298	20.423	
59 821	COMBO–0332443−273403	$03^{\rm h}32^{\rm m}44\overset{\rm s}{.}276$	$-27°34'03\overset{''}{.}31$	22.741	22.564	22.265	22.019	

$R = 22.93 \pm 0.02$ (no calibration errors included). There is still non-zero flux measured at the location of the transient object in February 2000 formally yielding $R = 25.41 \pm 0.19$, but it is not clear, whether the light originates from the outskirts of the neighboring galaxy or still from the Supernova.

In October it was measured on Oct. 10 with $V = 23.75 \pm 0.04$, on Oct. 13 with $B = 25.56 \pm 0.17$ and on Oct. 19 and 20 consistently with $R = 23.33 \pm 0.02$. Again, we can not decide on the B band sum frame with $1\overset{''}{.}2$ PSF whether the B flux is contributed from the galaxy or from the candidate. If it was a Supernova, the B measurement bracketed by V and R imaging could not be explained by variability. Therefore, the object must be unusually red with $B - V \gtrsim 1.8$ and it is not entirely clear whether the Supernova hypothesis can account for this color.

We note that the Supernova 1999gu reported by Cappellaro et al. (2000) and first observed with the WFI on Dec. 29, 1999 at $\alpha_{\rm J2000} = 3^{\rm h}33^{\rm m}00\overset{\rm s}{.}1$ and $\delta_{\rm J2000} = -27°51'40''$ in a galaxy at $z = 0.147$ is clearly visible in

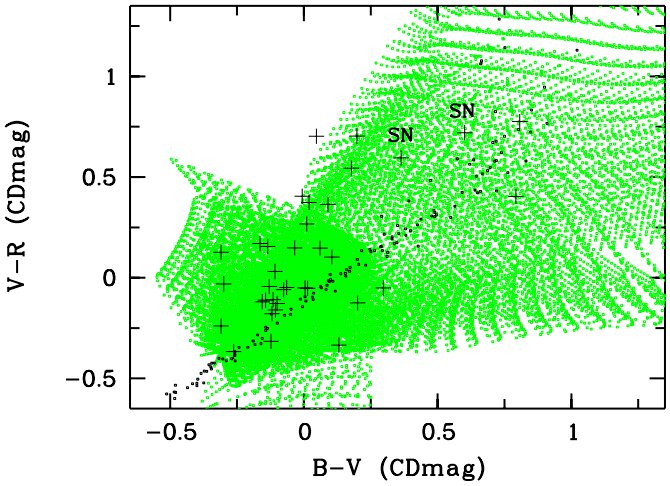

Fig. 9. Color-color diagram of variable objects (black crosses) compared with the expected stellar sequence (black dots) and a quasar color library (grey dots). Assuming the absence of short-term variability, most objects would be AGNs. Two Supernova (SN) candidates are within the limits of this diagram.

the images of February 2000 with $R = 21.5$, but since our object list was defined on the deep sum frame of October 1999, it is not contained in the catalogue presented here.

6. Summary and outlook

We have constructed a catalogue with positions, morphology and deep BVR photometry (B,$V_{5\sigma} \approx 25.5$ $R_{5\sigma} = 26$) of 63 501 objects on an area of $31\farcm5 \times 30'$ containing the Chandra Deep Field South. This catalogue is available to the scientific public at Centre de Données astronomiques de Strasbourg (CDS, `http://cdsweb.u-strasbg.fr/cgi-bin/qcat?J/A+A/377/442`).

We have presented a first list of faint variable objects, which are supposedly mostly quasars including some Seyfert galaxies or Supernovae in late stages. Three transient sources are strongly suggestive of supernovae, but one of them had an unusually red color of $B-V \gtrsim 1.8$.

When fully reduced, the dataset collected by the COMBO-17 survey will provide a bonanza of pseudo-spectroscopic information. We expect to classify some 50 000 objects over an area of 1 deg^2 down to $R \lesssim 24$ (completeness limit). Besides the classification infomation (star, galaxy or quasar) we will get spectral subclasses and high-quality redshift estimates for extragalactic sources. The full catalogue will then allow to finally classify also the variable sources and tell the redshifts of the Supernova host galaxies. It will not only provide an optical classification of the X-ray sources but also of neighboring objects in their environment.

Acknowledgements. This work was supported by the DFG–SFB 439. We would like to thank the referee, Dr. F. Mannucci for quite a detailed report which helped to improve the paper significantly.

References

Baade, D., Meisenheimer, K., Iwert, O., et al. 1998, The Messenger, 93, 13
Baade, D., Meisenheimer, K., Iwert, O., et al. 1999, The Messenger, 95, 15
Baade, D. 1999, ESO WFI User Manual, 21, Doc. No. LSO-MAN-ESO-22100-00001
Bertin, E., & Arnouts, S. 1996, A&AS, 117, 393
Bohlin, R., & Lindler, D. 1992, STScI Newsletter, 9, 19
Cappellaro, E., et al. 2000, IAU Circ., 7346
Francis, P. J., Hewett, P. C., Foltz, C. B., et al. 1991, ApJ, 373, 465
Giacconi, R., et al. 2000, AAS HEAD Meeting, 32, 07.01
Meisenheimer, K., et al. 2001, in preparation
Pickles, A. J. 1998, PASP, 110, 863
Röser, S., & Bastian, U. 1991, PPM Star Catalogue (Spektrum Akademischer Verlag, Heidelberg)
Röser, H.-J., & Meisenheimer, K. 1991, A&A, 252, 458
Wackermann, R. 1999, Diploma Thesis, Universität Heidelberg
Wisotzki L., Christlieb N., et al. 2000, A&A, 358, 77
Wolf, C., Meisenheimer, K., & Röser, H.-J. 2001a, A&A, 365, 660
Wolf, C., Meisenheimer, K., Röser, H.-J., et al. 2001b, A&A, 365, 681